

On the cyclic yield surface of some engineering materials under complex stress conditions

L. DIETRICH and Z. L. KOWALEWSKI (WARSZAWA)

THE PAPER PRESENTS a new method of mechanical parameters analysis. It deals with determination of a "cyclic yield surface" for selected engineering materials on the basis of cyclic curves experimentally obtained under a complex stress state. Location of the cyclic yield surface with respect to that of the initial yield locus may constitute the basis for evaluation of the material sensitivity to the cyclic deformation. Tests have been carried out with the use of PA6 aluminium alloy and 18G2A low-alloy steel, both in the as-received state. The experimental programme was the same for both considered materials. Firstly, an initial yield surface was determined using a number of specimens which were loaded up to the plastic range along different loading paths. Secondly, cyclic predeformations due to various loading paths in the plane stress state were induced by cyclic loading at ambient temperature under constant ($\Delta\varepsilon = \pm 0.65\%$) and gradually decreasing strain amplitude (from $\Delta\varepsilon = \pm 0.65\%$ to 0%). Finally, subsequent yield surfaces were determined using the single specimen method. It is shown that depending on the material, a cyclic loading induces softening (low-alloy steel) or hardening (aluminium alloy) effect in the strain range considered. All differences in material responses to cyclic prestraining for the tested materials are discussed in detail.

1. Introduction

SOLVING THE PROBLEMS associated with a variation of material properties due to cyclic loading inducing permanent deformation of the construction is regarded as one of the most important tasks of the plasticity theory [1-19]. A rapid progress observed nowadays in this area deals directly with the qualitative changes in the experimental technique, i.e. with development of both the computer systems enabling us to control the multiaxial testing machines working in the closed loop of feedback, and digital registration of experimental results together with their further conversion, using more powerful computers and novel software.

The steady-state cyclic deformation resistance of a material is usually described on the basis of the cyclic stress-strain curve [2]. According to the definition of the cyclic stress-strain curve, it is the locus of tips of the stable hysteresis loops from several companion tests at different, completely reversed constant strain amplitudes. Such a steady-state "stress amplitude - strain amplitude" curve is often compared with the monotonic stress-strain curve, Fig. 1. Depending on the mutual location of these curves, the cyclically induced changes in deformation resistance can be identified, i.e. softening if the cyclic curve is below the monotonic curve, and hardening if the cyclic curve lies above the monotonic curve.

Some materials are insensitive to the cyclic deformation and, as a consequence, in these cases the cyclic curve does not differ from the monotonic one.

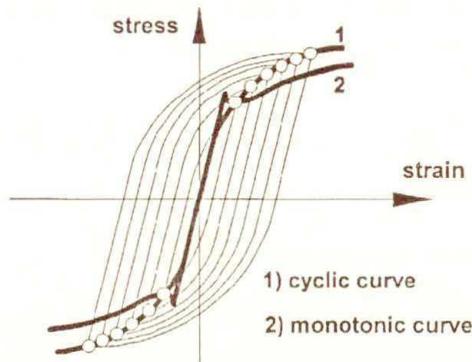


FIG. 1. Comparison of a typical cyclic and monotonic curves.

According to the definition given above, the cyclic stress-strain curve is obtained by connecting the tips of the stable hysteresis loops from several separate tests carried out at different, completely reversed strain ranges. Each test is performed at a constant strain amplitude. The loop can be achieved for some materials after several cycles. For the others, however, approximately half their fatigue life is required. Since this method requires a number of testpieces and relatively long testing time, it is rarely used in practice. To overcome these inconveniences, alternative procedures for determining the cyclic curves using only a single specimen are applied. The most known tests, described in detail by MORROW [1], are as follows:

- (A) Multiple step tests,
- (B) Incremental step tests,
- (C) Monotonic tension after cyclic straining,
- (D) Individual hysteresis loop,
- (E) Decremental test.

The last method is regarded as the fastest and the most effective. It requires to load a specimen to a stable hysteresis loop under cycling loads at selected constant strain amplitudes, followed by cycling with a gradually decreasing strain amplitude up to the zero level. A number of cycles with a gradually decreasing strain amplitude should be sufficient to determine the cyclic curve with desired accuracy. Such a method was successfully used by LAMBA and SIDEBOTTOM [8] to obtain cyclic curves under nonproportional loading. The method was also applied to determine cyclic curves for different proportional cyclic loading paths in the strain space considered.

The main aims of the experimental project, the results of which are presented in the paper, were threefold. Firstly, it had to give an answer to the question: how

a plastic prestrain induced in metals during manufacturing processes of semifinished elements may change their mechanical properties. Secondly, the programme of tests had to determine up to what degree the known deformation history under cyclic loading may change the original anisotropy of the tested materials, and the third aim of the project was to determine a "cyclic yield surface" for the selected ranges of plastic deformation, on the basis of cyclic curves experimentally obtained under a complex stress state. The cyclic yield surface reflects the material ability to hardening or softening due to cyclic loading in different directions of the (σ_{xx}, τ_{xy}) stress plane. Although the cyclic yield surface does not describe the mechanical properties of a material subject to cyclic straining in an arbitrarily chosen direction, it may be treated as an envelope of the yield surfaces for a material subject to prior cyclic deformation in various directions. Its location with respect to that of the initial yield locus may constitute the basis for evaluation of the material sensitivity to the cyclic deformation.

2. Experimental details

Tests have been carried out with the use of low-alloy steel and aluminium alloy, both in the as-received state. Notations of these materials according to Polish Standards as well as their chemical composition are given in Table 1 and Table 2. According to ISO Standards 4950/2-1981, the chemical composition of the steel in question corresponds to that of the high yield strength steel with grade E355.

Table 1. Chemical composition of the 18G2A low-alloy steel manufactured according to Polish Standards.

	C	Mn	Si	P_{\max}	S_{\max}
	[%]	[%]	[%]	[%]	[%]
18G2A	max 0.2	1.0 – 1.5	max 0.55	0.04	0.04

Table 2. Chemical composition of the PA6 aluminium alloy manufactured according to Polish Standards.

	Cu	Mg	Mn
	[%]	[%]	[%]
PA6 aluminium alloy	3.8 – 4.8	0.4 – 1.1	0.4 – 1.0

All tests were carried out on tubular thin-walled specimens, manufactured from rods of 45 [mm] diameter. In the case of steel, the rods were manufactured

by rolling, whereas those for aluminium alloy – by extrusion. An engineering drawing of the specimen is shown in Fig. 2.

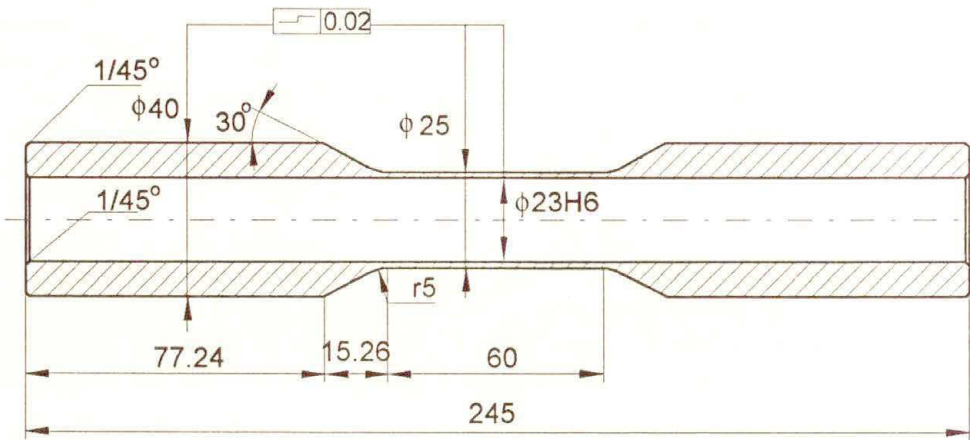


FIG. 2. Dimension of the specimen.

All experiments reported in this paper were carried out with the use of the INSTRON electrohydraulic, closed-loop, servo-controlled, biaxial testing machine enabling combined loading in tension – compression – torsion – reverse torsion.

The strains were measured by means of strain gauge rosettes bonded to the outer surface of the specimen on its gauge length. More details concerning the experimental procedure are given in [17].

3. Experimental programme

The experimental programme for both materials comprised three steps.

Firstly, an initial yield surface was determined for each material. In order to determine the initial yield surface, eight specimens were selected, each of them was loaded with different ratios of stress components in the two-dimensional stress space (σ_{xx}, τ_{xy}). In the next step of the experimental programme, prior deformation of specimens by means of proportional cyclic loading in selected directions of the (σ_{xx}, τ_{xy}) stress plane was carried out. The prestraining programme comprised two stages:

(1) cyclic loading for constant amplitude of total effective strain $\Delta\varepsilon = \pm 0.65\%$,

(2) cyclic loading with gradually decreasing total effective strain amplitude from $\Delta\varepsilon = \pm 0.65\%$ to $\Delta\varepsilon = \pm 0.0\%$.

The programme of constant strain amplitude cycles included 81 quarter-cycles. It was used to achieve the saturation cycle.

The programme of cyclic loading with decreasing strain amplitude comprised 30 full cycles. It followed just after the constant amplitude cycles were carried out, and was applied in order to determine cyclic curves.

For both materials eight different strain paths were considered, Fig. 3. These

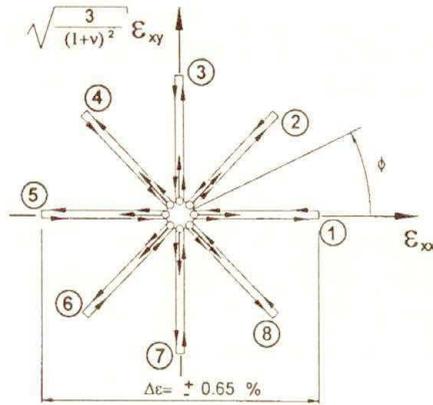


FIG. 3. Proportional cyclic loading paths for prestraining the materials.

paths were obtained by cyclic loading under strain control mode. Denotation of the vertical axis in Fig. 3 contains Poisson’s ratio ν which for both materials was not equal to 0.5 in the strain range considered in the programme. The experimentally determined Poisson’s ratios for the steel and aluminium alloy were equal to 0.34 and 0.30, respectively.

When the cyclic prestraining process of each specimen was completed, determination of the subsequent yield surface was performed on the INSTRON testing machine with the use of the single-specimen method, Fig. 4. In this technique a

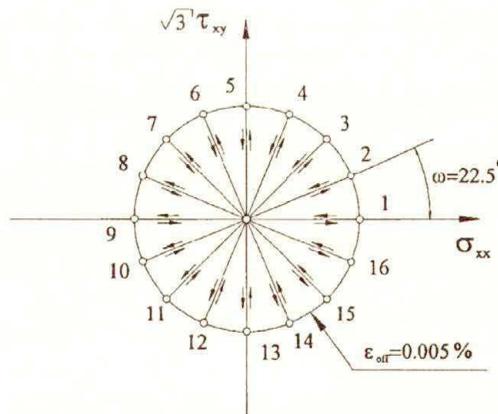


FIG. 4. Loading sequence for yield locus determination using single-specimen method.

specimen was loaded along various loading paths, each time until some measurable and limited plastic strain was observed (in our case the offset strain equal to $\varepsilon_{\text{off}} = 5 \times 10^{-5}$ was selected as the yield point). At each yield point the specimen was unloaded and again loaded in another direction until the entire yield locus was obtained. These directions varied from each other by a chosen angular increment assumed to be 22.5° . The experimental procedure comprised 16 points determined from the selected proportional loading paths. In Fig. 4 the increasing numbers at the yield points indicate the loading sequence.

4. Yield condition

SZCZEPIŃSKI [21] has proposed, on the basis of the Mises anisotropic yield condition [20], more general form of the yield condition for materials displaying the Bauschinger effect and rotation of the yield locus axes with respect to the coordinate system. That yield condition has been adopted in numerical calculations presented in the paper.

Generally, the Mises anisotropic yield condition in the form derived by Szczepiński can be expressed by the following relationship [21]:

$$\begin{aligned}
 (4.1) \quad f(\sigma_{ij}) = & k_{12}(\sigma_{xx} - \sigma_{yy})^2 + k_{23}(\sigma_{yy} - \sigma_{zz})^2 + k_{31}(\sigma_{zz} - \sigma_{xx})^2 \\
 & + 2\tau_{xy} [k_{16}(\sigma_{zz} - \sigma_{xx}) + k_{26}(\sigma_{zz} - \sigma_{yy})] \\
 & + 2\tau_{yz} [k_{24}(\sigma_{xx} - \sigma_{yy}) + k_{34}(\sigma_{xx} - \sigma_{zz})] \\
 & + 2\tau_{zx} [k_{35}(\sigma_{yy} - \sigma_{zz}) + k_{15}(\sigma_{yy} - \sigma_{xx})] \\
 & - 2k_{45} \cdot \tau_{yz} \cdot \tau_{zx} - 2k_{56} \cdot \tau_{zx} \cdot \tau_{xy} - 2k_{64} \cdot \tau_{xy} \cdot \tau_{yz} \\
 & + k_{44} \cdot \tau_{yz}^2 + k_{55} \cdot \tau_{zx}^2 + k_{66} \cdot \tau_{xy}^2 \\
 & - b_{12}(\sigma_{xx} - \sigma_{yy}) - b_{23}(\sigma_{yy} - \sigma_{zz}) - b_{31}(\sigma_{zz} - \sigma_{xx}) \\
 & + b_{44} \cdot \tau_{yz} + b_{55} \cdot \tau_{zx} + b_{66} \cdot \tau_{xy} = 1.
 \end{aligned}$$

In our experimental project, the tests have been performed under plane stress conditions for which only σ_{xx} and τ_{xy} were not equal to zero. When this is substituted into the relation (4.1), the yield condition simplifies as follows:

$$\begin{aligned}
 (4.2) \quad f(\sigma_{ij}) = & (k_{12} + k_{31})\sigma_{xx}^2 - 2 \cdot k_{16} \cdot \tau_{xy} \cdot \sigma_{xx} + k_{66} \cdot \tau_{xy}^2 \\
 & + (b_{31} - b_{12})\sigma_{xx} + b_{66} \cdot \tau_{xy} = 1,
 \end{aligned}$$

where coefficients k_{ij} , b_{ij} are functions of the yield limits determined from experiments at tension, compression, torsion, and reverse torsion tests.

Expression (4.2) represents the equation of a curve of second order, usually written in the form:

$$(4.3) \quad A\sigma_{xx}^2 + 2B\sigma_{xx}\tau_{xy} + C\tau_{xy}^2 + 2D\sigma_{xx} + 2F\tau_{xy} = 1,$$

where coefficients A and D denote functions of the yield limits at tension and compression. The coefficients C and F are related to the shear yield limits obtained from the tests under torsion and reverse torsion.

The B coefficient, which is proportional to the rotation of a yield surface with respect to (σ_{xx}, τ_{xy}) co-ordinate system, has no such simple physical interpretation as the coefficients described above, and it cannot be deduced from uniaxial tests. In order to find its value it is necessary to carry out at least one test in a complex stress state.

The yield condition in form (4.3) is determined by five material parameters which can be identified with such ellipse parameters as lengths of its axes, co-ordinates of ellipse centre, and rotation angle with respect to the co-ordinate system.

5. Experimental results

5.1. Results for the materials in the as-received state

Initial yield surfaces for aluminium alloy and low-alloy steel, both in the as-received state, obtained for the offset $\varepsilon_{\text{off}} = 5 \times 10^{-5}$, are shown in Fig. 5 and

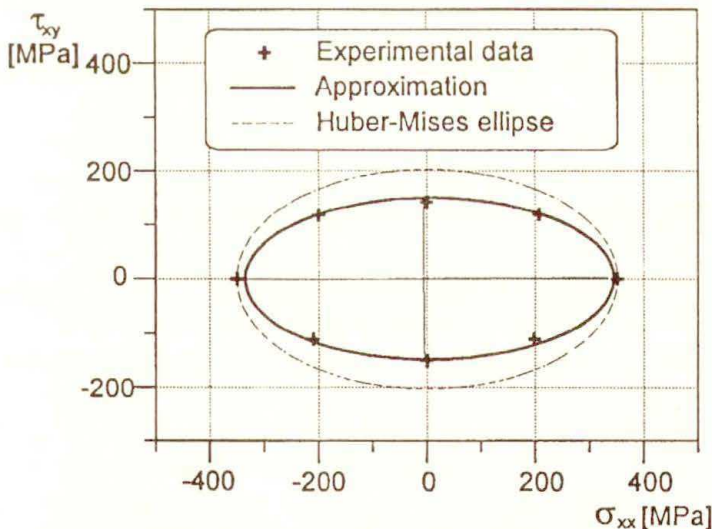


FIG. 5. Experimental points and fitted yield surface, Eq. (4.3), for the as-received aluminium alloy.

Fig. 6, respectively. Points in these figures represent experimental results while ellipses are determined by the least squares evaluation of the A , B , C , D , F coefficients in equation (4.3).

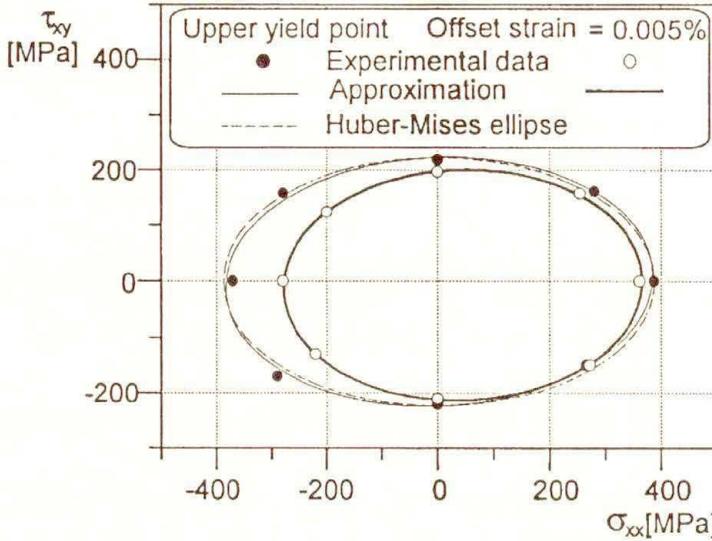


FIG. 6. Experimental points and fitted yield surfaces, Eq. (4.3), for the as-received low-alloy steel.

It is seen that the materials in the as-received state exhibit certain initial anisotropy which can be clearly identified by comparison of the experimental results with predictions obtained using the isotropic Huber-Mises yield condition. In both figures the Huber-Mises ellipses are plotted by broken lines.

In the case of aluminium alloy, an initial anisotropy is reflected by flattening of the theoretical yield surface calculated using the isotropic Huber-Mises yield condition.

Similarly to the aluminium alloy, also the low-alloy steel tested exhibits anisotropic behaviour in the as-received state. In this case, however, the effect manifests itself by the shift of the yield surface in the direction of tension.

The steel tested indicated upper and lower yield limits. The observations of the upper and lower yield points did not confirm an anisotropy of the mechanical properties of the steel observed for the assumed yield offset. In Fig. 6, besides the yield locus for the assumed offset strain, also the yield surface corresponding to the upper yield limit is presented. That surface was built on the basis of the "effective stress - effective strain" diagrams representing eight different directions in the two-dimensional stress space (σ_{xx}, τ_{xy}) . As it is clearly shown, the upper yield point surface does not exhibit anisotropic effects. Hence, it can be described accurately by the isotropic Huber-Mises yield condition (ellipse plotted by

broken line in Fig. 6). However, it has to be noted that for each direction under consideration, the upper yield point corresponds to a different strain level. In other words, the ellipse reflecting the upper yield points obtained for various loading combinations does not represent any yield definition. Mutual location of the yield surfaces presented in this figure reveals a certain form of the anisotropy of the steel.

Summing up all of these remarks, it can be stated that both materials exhibit anisotropic properties in the as-received state coming from the industrial forming processes. In the case of steel however, we can observe isotropic properties in the sense of the upper yield limit, but the courses of the stress-strain characteristics up to the upper yield point for various loading paths tested in the programme are not coincident, identifying in this manner anisotropic character of the material in the strain range under consideration.

5.2. Results for the materials prestrained due to cyclic loading

The second step of the experimental procedure comprised the cyclic deformation carried out under constant strain amplitude with the objective to attain a saturated cyclic state, and cyclic deformation with gradually decreasing strain amplitude in order to obtain cyclic curves. An example of this process in case of torsion - reverse torsion cycles of aluminium alloy is presented in the Fig. 7a. The stress response onto the deformation programme given in Fig. 7a is shown in Fig. 7b.

In Fig. 7c the results for the cyclic loading with constant strain amplitude are illustrated in the form of the stress-strain diagram. As it is clearly seen, the saturation cycle was not achieved for the assumed programme of constant cyclic loading. The same effect was also observed for the remaining tests carried out for other directions of cyclic loadings.

Just after the constant strain amplitude cycles were carried out, the programme of cyclic loading with decreasing strain amplitude followed. An example of a typically observed stress response due to this part of programme is shown in Fig. 7d. The results in the form of a stress-strain diagram for the cyclic loading with decreasing strain amplitude illustrate the method for determination of the cyclic curve as a set of tips of the loops for cycles with decreasing strain amplitude. The results shown in this figure are plotted in the stress - total strain diagram. Using the DADiSP software, they can be automatically converted to a diagram of stress against plastic strain. Such transformation is presented in Fig. 7e.

In order to show how the initial anisotropy influences the response of the material to cyclic loading, the results for another loading path (tension - compression cycles) are presented in Figs. 8a, b, c, d. The sequence of figures is similar to that in the Figs. 7b, c, d, e, i.e. in Fig. 8a a stress response to the programme shown in Fig. 7a is presented, the stress response for constant strain amplitude cycling is

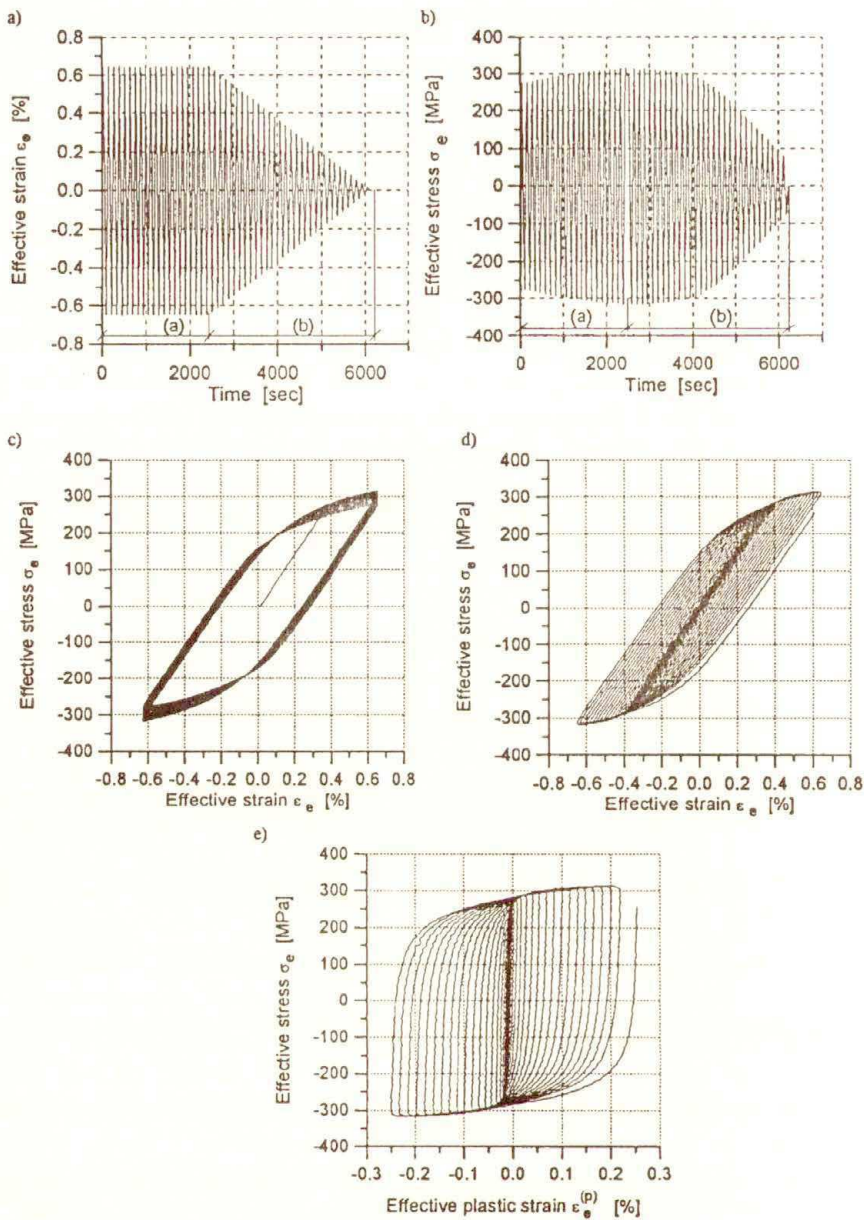


FIG. 7. a) Programme of cyclic loading for aluminium alloy (cycling in torsion-reverse torsion). b) Stress response to the strain-controlled cyclic loading shown in Fig. 7a. c) Stress response to the strain-controlled cyclic loading with constant strain amplitude. d) Stress response to the strain-controlled cyclic loading with decreasing strain amplitude. e) Stress - plastic strain diagram of the stress response to the programme of cyclic loading with decreasing strain amplitude.

shown in Fig. 8b. Figure 8c presents the stress response to the cyclic programme with gradually decreasing strain amplitude, and Fig. 8d shows the same results after subtraction of the elastic strain. It has to be noted that the width of the loops obtained during tension-compression cycles are significantly smaller than the loops achieved during cycling in torsion-reverse torsion (compare Figs. 7e and 8d).

The results for the steel in the case of cycling in tension-compression are demonstrated in Figs. 9 a, b, c, d, e. Again the stress response to the deformation programme given in Fig. 9a is shown in Fig. 9b. In the next figure (Fig. 9c), the

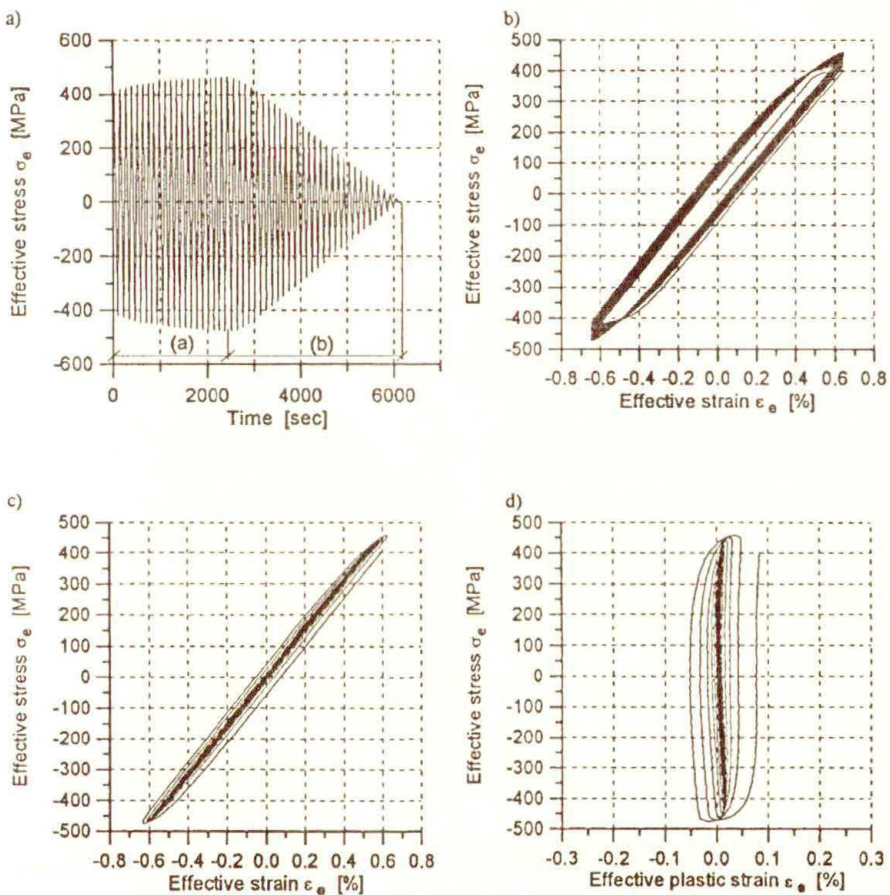


FIG. 8. Stress responses to cyclic loading of aluminium alloy (cycling in tension-compression). a) Stress response to the strain-controlled cyclic loading shown in Fig. 7a. b) Stress response to the strain-controlled cyclic loading with constant strain amplitude. c) Stress response to the strain-controlled cyclic loading with decreasing strain amplitude. d) Stress - plastic strain diagram of the stress response to the programme of cyclic loading with decreasing strain amplitude.

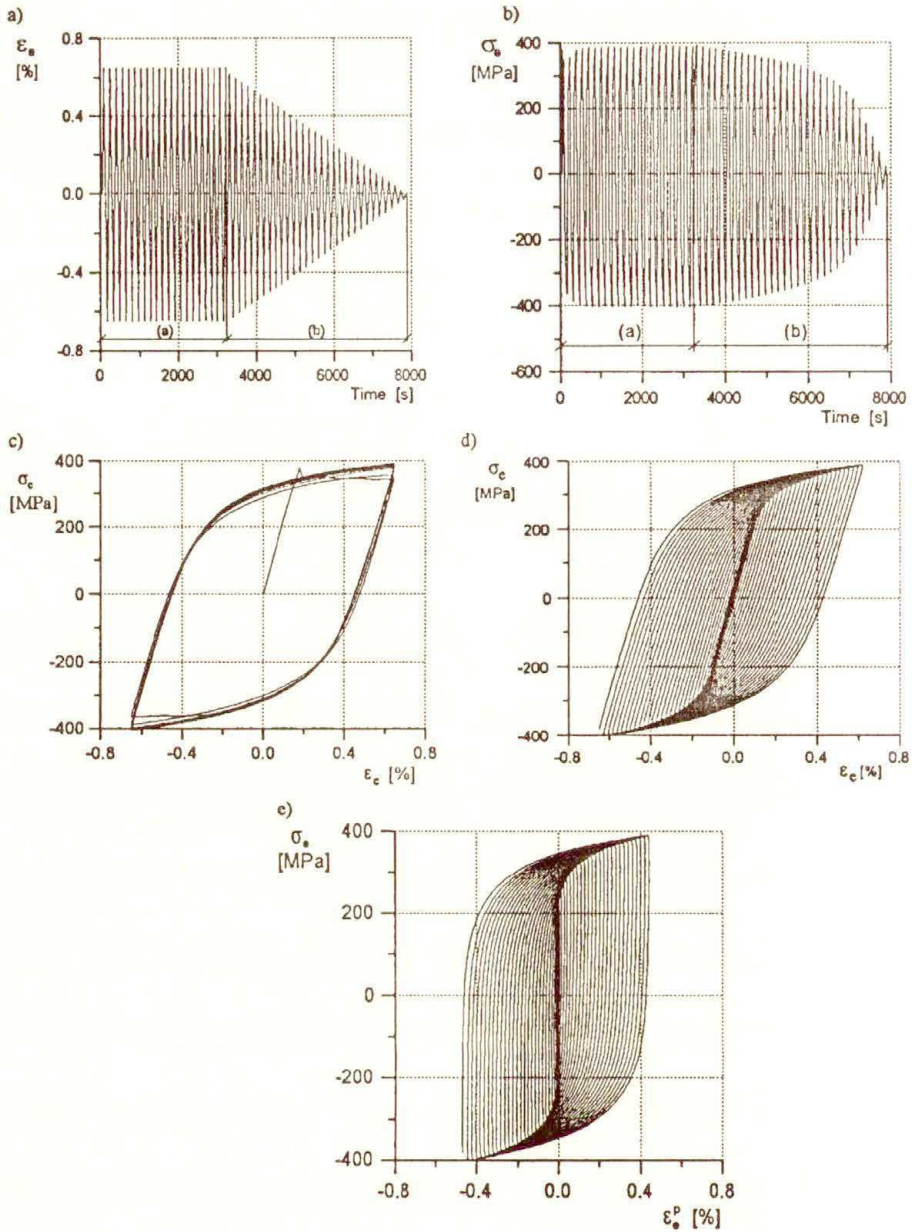


FIG. 9. a) Programme of cyclic loading for low-alloy steel (cycling in tension-compression). b) Stress response to the strain-controlled cyclic loading shown in Fig. 9a. c) Stress response to the strain-controlled cyclic loading with constant strain amplitude. d) Stress response to the strain-controlled cyclic loading with decreasing strain amplitude. e) Stress - plastic strain diagram of the stress response to the programme of cyclic loading with decreasing strain amplitude.

results for the cyclic loading with constant total strain amplitude are illustrated in the form of the stress-strain diagram. As it is clearly seen, the saturation cycle was achieved for the assumed programme of constant strain amplitude cycling relatively quickly, since it required only five full cycles. The same effect was also achieved for the remaining tests carried out for other directions of cyclic loadings. An example of a typically observed stress response due to the programme of cyclic loading with decreasing strain amplitude is shown in the next two diagrams. In Fig. 9d, the stress versus total strain is presented, whereas in Fig. 9e a diagram of stress versus plastic strain is shown.

In the case of the steel, independently of the cyclic loading paths considered, no essential differences in the width of the loops were observed, what distinguishes the results from those obtained for aluminium alloy.

The cyclic curves for aluminium alloy determined for all directions of cyclic deformation are compared in Fig. 10. All these curves exhibit different courses

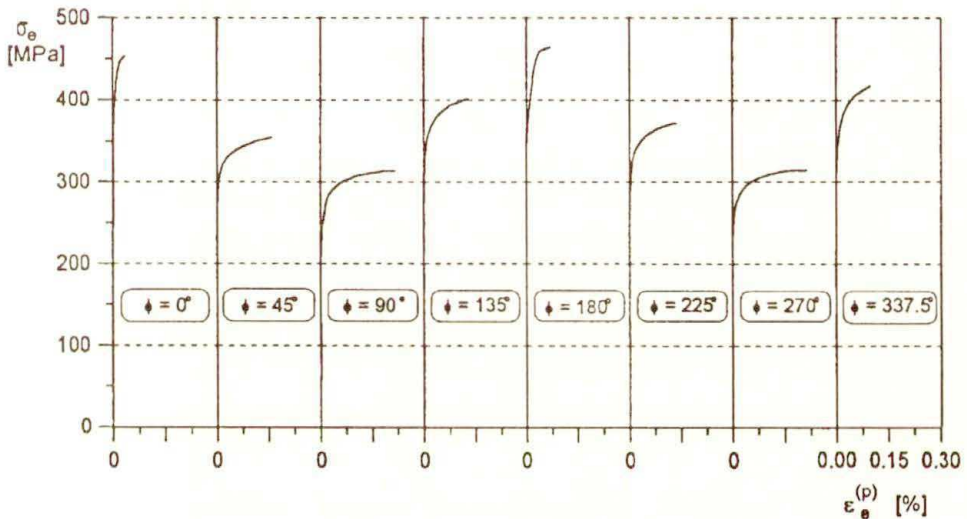


FIG. 10. Stress-strain curves of aluminium alloy for various directions of proportional cyclic loading.

and shapes. On the basis of cyclic curves, the cyclic yield locus has been determined, Fig. 11. Such a surface represents the ability of the material to variation of mechanical parameters due to cyclic deformation for different orientations in the plane stress state. It has been determined for the same yield offset as that used to obtain the initial yield surface ($\epsilon_{\text{off}} = 5 \times 10^{-5}$) in order to enable their comparison. Comparative studies of the shapes and dimensions of the initial and cyclic yield surfaces, Fig. 11, show that the history of cyclic deformation in the plastic range induces hardening of the material. It is interesting to note that the greatest hardening was achieved in the directions of tension and compression

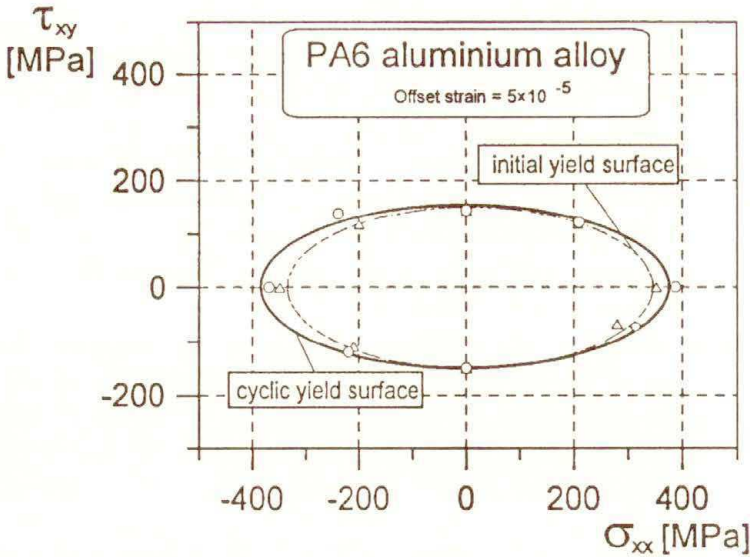


FIG. 11. Comparison of the cyclic yield surface with the initial yield locus for aluminium alloy.

while the smallest hardening was observed in the direction coincident with that of the initial anisotropy resulting from the forming processes (this direction corresponds to torsion-reverse torsion). It is clear that the initial anisotropy was not forgotten due to the cyclic process.

The cyclic curves for the steel determined for all directions of cyclic deformation are compared in Fig. 12. Contrary to the results for aluminium alloy, all

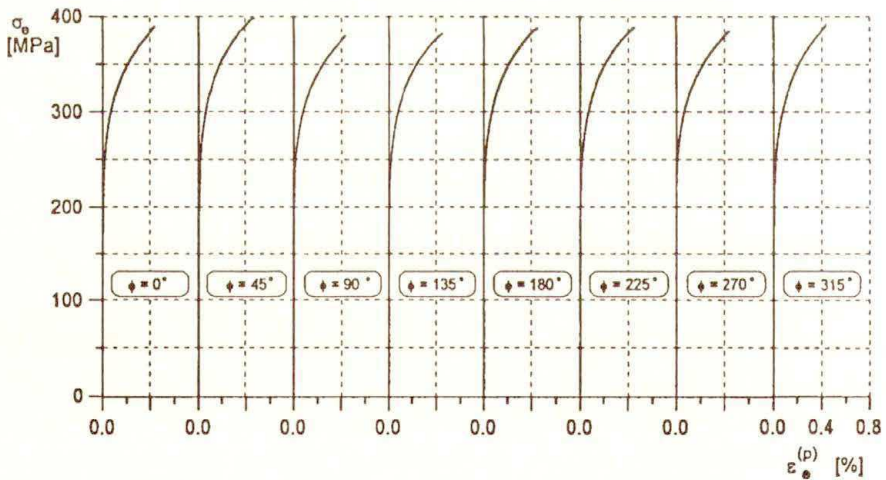


FIG. 12. Stress-strain curves of low-alloy steel for various directions of proportional cyclic loading.

these curves show a similar course and shape, especially at low level of the plastic strain (up to 0.01%). Here again, on the basis of cyclic curves, the cyclic yield locus has been determined, Fig. 13. Since the cyclic yield surface has been obtained for the same yield offset as that used to obtain the initial yield surface, it is easy to compare them and formulate the concluding remarks. Analysis of the shapes and dimensions of the initial and cyclic yield surfaces proves that the history of cyclic deformation in the plastic range for all directions induced softening of the material. It is interesting to note that, independently of the anisotropy observed in the as-received material, the centre of the cyclic yield locus is located in the origin of the co-ordinate system. Hence, it can be concluded that in steel, an initial anisotropy was forgotten due to the cyclic process, and the material exhibits a memory for the prestress induced during cyclic deformation.

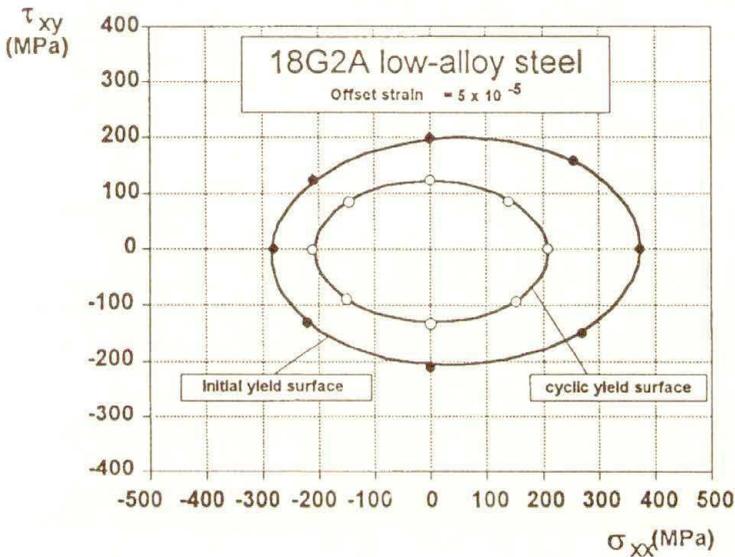


FIG. 13. Comparison of the cyclic yield surface with the initial yield locus for low-alloy steel.

After cyclic predeformation, yield surfaces for selected offset strain were determined by the technique of sequential probes of the single specimen. All yield surfaces determined for aluminium alloy after cyclic loading along selected proportional paths are shown in Fig. 14 for the offset strain equal to 5×10^{-5} . They are compared with the initial yield surface, plotted in the middle of Fig. 14, for the same offset strain. Numbers from 1 to 8 denote the data obtained for the material after different proportional cyclic loading paths, the orientation of which was described by $\phi = 0^\circ; 45^\circ; 90^\circ; 135^\circ; 180^\circ; 225^\circ; 270^\circ; 315^\circ$, respectively (cf. with Fig. 3). Points in Fig. 14 denote experimental results, while ellipses represent the best fit obtained by using equation (4.3). Yield surfaces, of the same offset,

for the aluminium alloy prestrained due to cyclic loading have significantly greater dimensions in comparison to those for the initial yield surface. This means that the aluminium alloy tested after cold work exhibits hardening effect in the strain range considered. Since the evolution and mutual location of the yield loci are not clearly reflected in Fig. 14, they are compared together in Fig. 15a, b. In

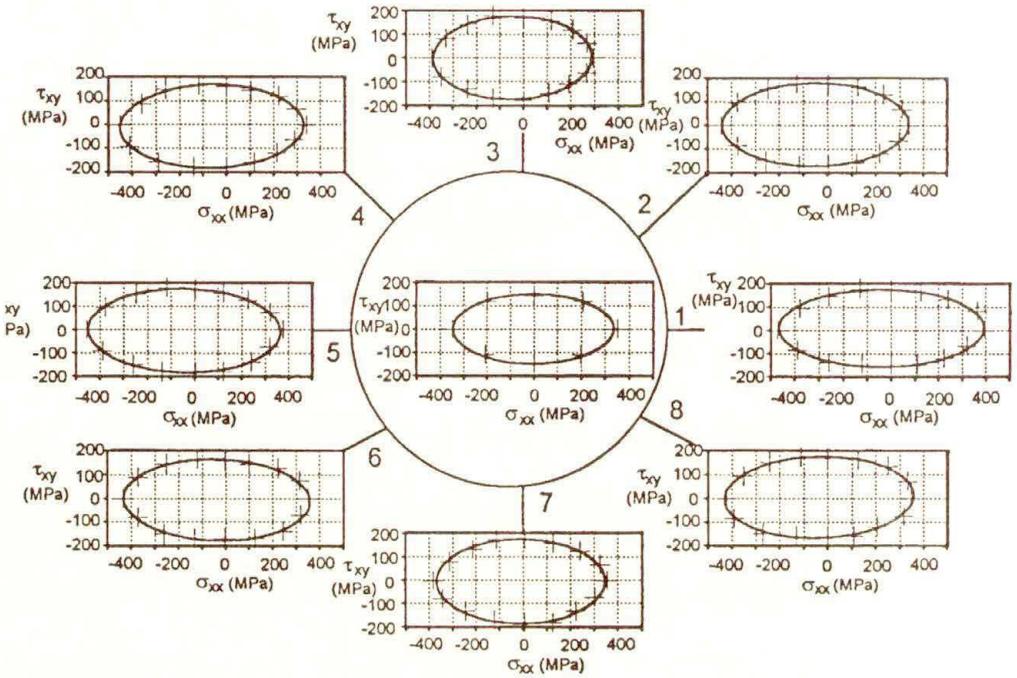
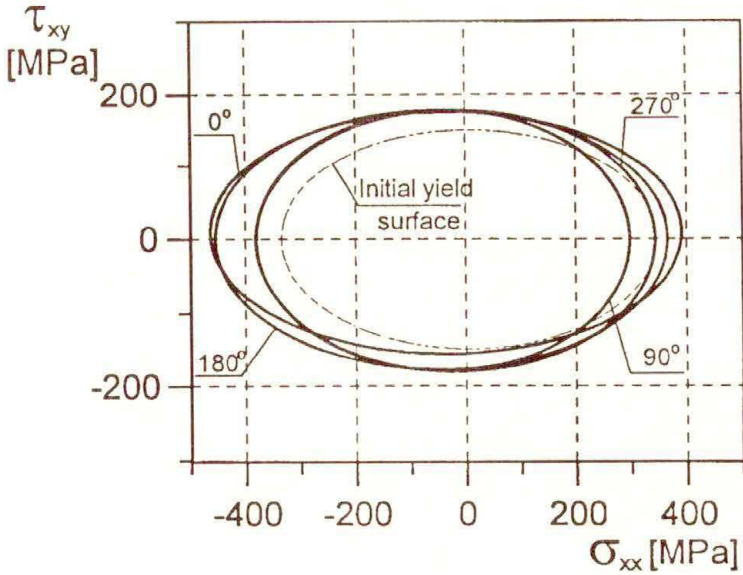


FIG. 14. Experimental points and fitted yield surfaces for aluminium alloy prestrained due to cyclic loading along various proportional paths, offset strain 5×10^{-5} .

order to keep clear view, the data points in Fig. 15a, b are omitted. Numbers in both figures denote orientations of the proportional cyclic loading paths. Shown in Fig. 15a are yield surfaces for the material prestrained due to cyclic loading in directions described by $\phi = 0^\circ$; $\phi = 90^\circ$; $\phi = 180^\circ$; $\phi = 270^\circ$, whereas in Fig. 15b are shown subsequent yield surfaces for the remaining cyclic loading paths considered in the experimental programme. The shape analysis of these yield surfaces leads to the conclusion that the dimensions of yield locus are dependent on the direction of cyclic preloading. The greatest hardening effect was achieved in the tension and compression directions. It is shown that the sense of the loading direction in the first cycle for the chosen direction changes solely the location of the yield locus centre without any other visible differences, especially in the shape and dimensions of the surface. It was confirmed for all the directions examined.

a)



b)

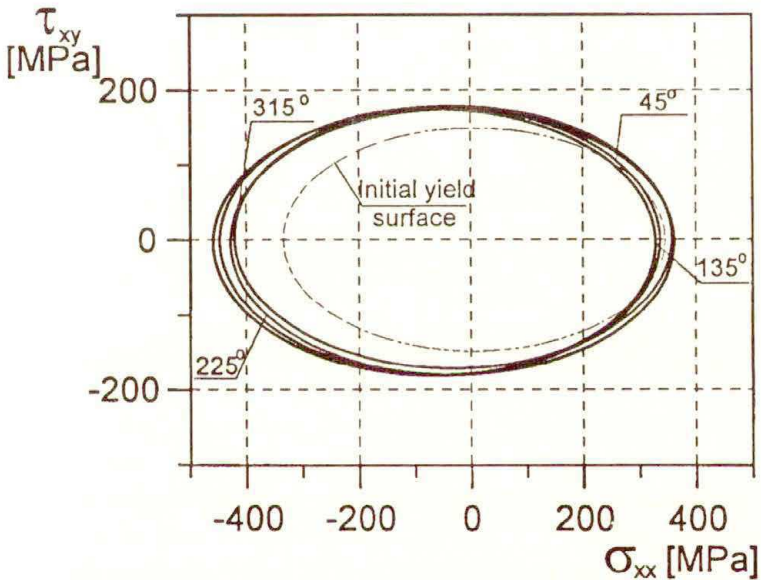


FIG. 15. Comparison of the initial yield surface with subsequent yield loci (aluminium alloy) a) after prestraining due to cyclic loading along the following proportional strain paths: 0° , 90° , 180° , 270° , offset strain 5×10^{-5} ; b) after prestraining due to cyclic loading along the following proportional strain paths: 45° , 135° , 225° , 315° , offset strain 5×10^{-5} .

In the next two figures are shown the results for steel. In Fig. 16 are presented experimental points together with ellipses reflecting the shapes and dimensions of the subsequent yield surfaces which have been determined using the yield

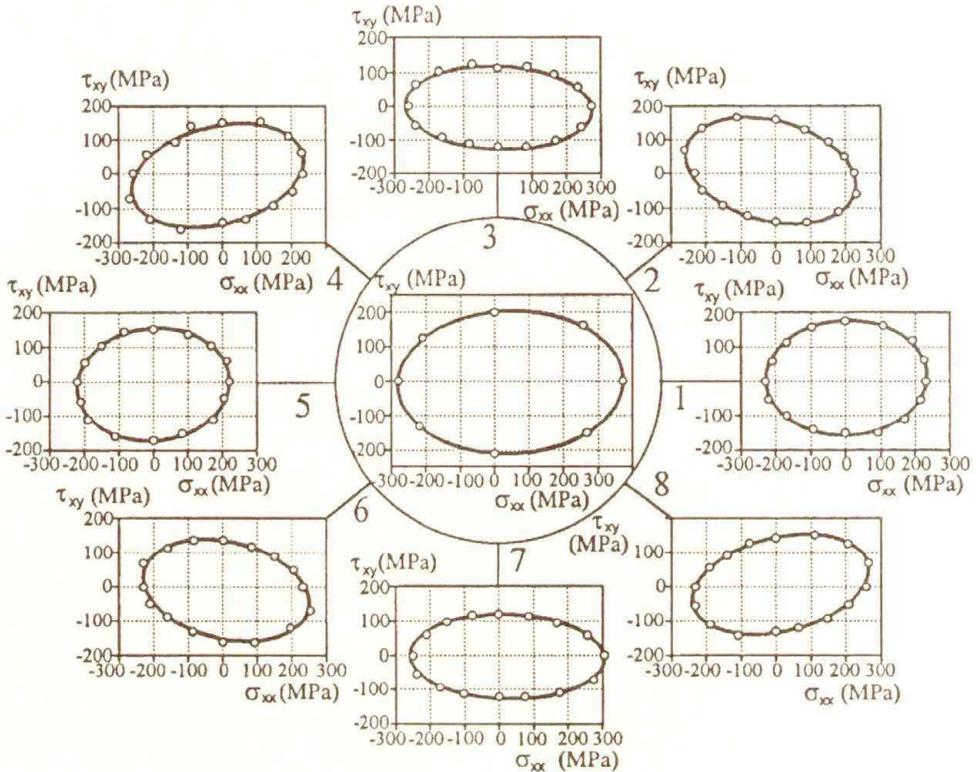
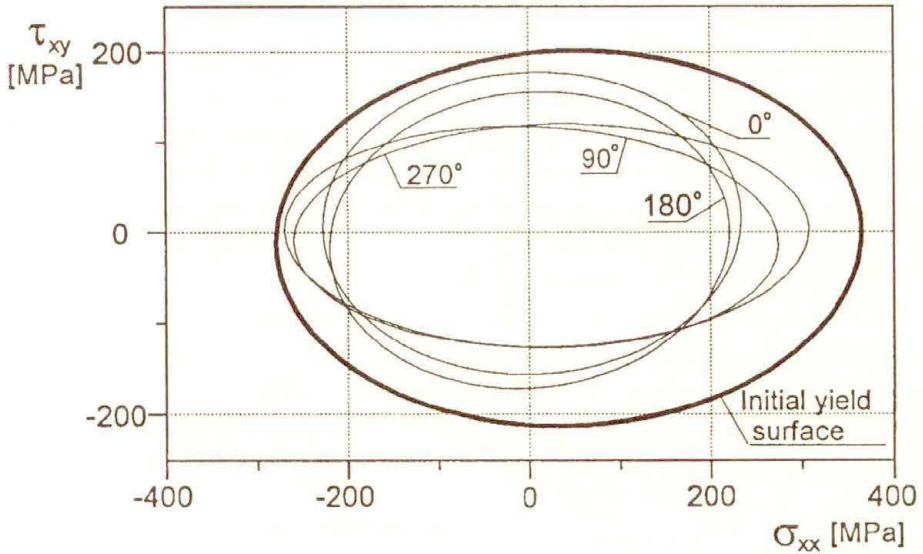


FIG. 16. Experimental points and fitted yield surfaces for the steel prestrained due to cyclic loading along various proportional paths, offset strain 5×10^{-5} .

condition in the form of equation (4.3). As it is clearly seen, a good agreement is achieved between the experimental data and the results following from the approximation. Similarly to the data analysis of aluminium alloy, in order to enable accurate assessment of the steel yield loci variations, in Fig. 17 a, b are shown subsequent yield surfaces at one co-ordinate system without experimental points. They are compared with the initial yield surface (bold line) for the same offset strain ($\epsilon_{\text{off}} = 5 \times 10^{-5}$). Again numbers in both figures denote orientation of the proportional cyclic loading paths. Yield surfaces, of the same offset strain, for the steel prestrained due to cyclic loading have significantly smaller dimensions in comparison to those for the initial yield surface, so they are located within it. This means that the low-alloy steel tested after cyclic cold work exhibits softening effect in the strain range considered. The shape analysis of these yield surfaces

a)



b)

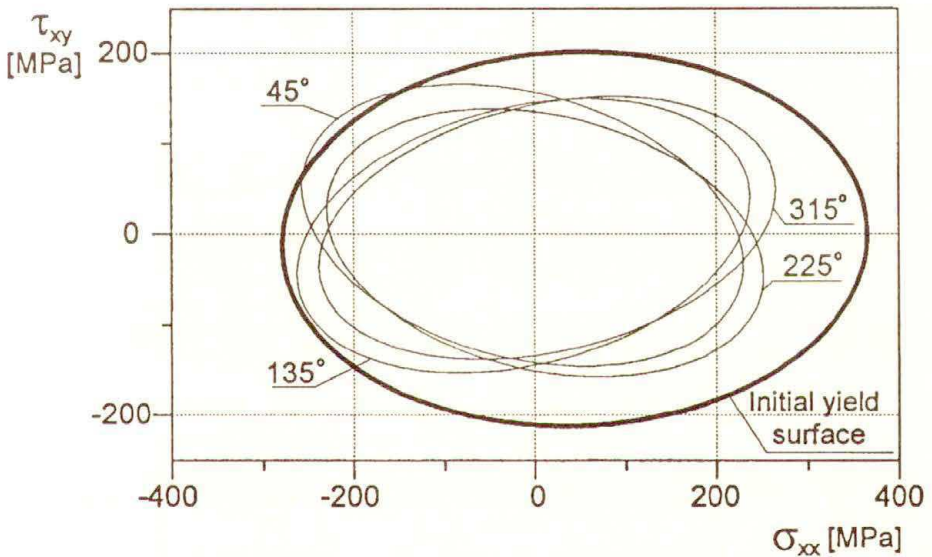


FIG. 17. Comparison of the initial yield surface with subsequent yield loci (low-alloy steel) a) after prestraining due to cyclic loading along the following proportional strain paths: 0° , 90° , 180° , 270° , offset strain 5×10^{-5} ; b) after prestraining due to cyclic loading along following proportional strain paths: 45° , 135° , 225° , 315° , offset strain 5×10^{-5} .

leads to the conclusion that the dimensions of yield locus are dependent on the direction of cyclic preloading. The greatest softening effect was always achieved in the direction which was coincident with that used in the preliminary cyclic deformation. The effect of the cyclic loading sense in the first cycle is clearly illustrated in Fig. 17a for example for $\phi = 90^\circ$ and $\phi = 270^\circ$. It is shown that the sense of the loading direction in the first cycle for the chosen direction changes solely the location of the yield locus centre without any other visible differences. It was observed for all the directions examined.

More accurate analysis concerning the degree of the prestraining effect can be attained on the basis of graphical illustrations of the variation of yield surface dimensions as a function of the predeformation direction. The variation of the major and minor semi-axes of the subsequent yield surfaces for the steel due to cyclic prestraining is shown in Fig. 18 as a function of cyclic loading direction.

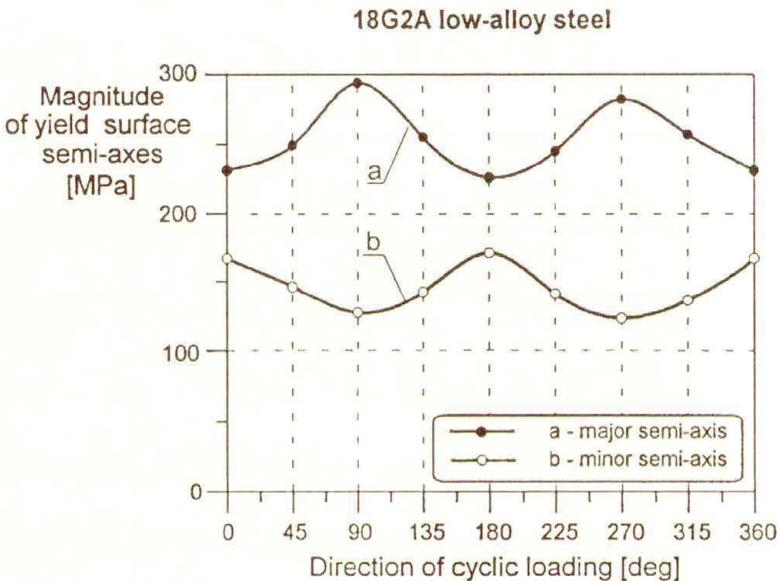


FIG. 18. Variations of the major and minor semi-axes of subsequent yield surfaces for the steel.

The same diagram for the aluminium alloy is presented in Fig. 19. From these diagrams it can be observed how the cyclic deformation changes basic dimensions of the yield surface.

The major semi-axis of the initial yield surface for steel was equal to 326 MPa, while the minor one was equal to 204 MPa. The same dimensions for the aluminium alloy were 341 MPa and 150 MPa, respectively.

The effect of softening is clearly demonstrated for the steel in Fig. 18. The maximum softening observed for this material was achieved for those directions

which were coincident with the cyclic ones. Moreover, a confirmation of the conclusion that for the selected proportional loading path, the degree of softening was not sensitive to the sense of loading, can be easily found. For example, the degree of softening for the “positive torsion-negative torsion” direction was almost the same, independently of the sense of cyclic process initiation, i.e. the positive torsion (90°) or the negative torsion (270°). The smallest softening effect was observed for the direction perpendicular to that at the cyclic loading used.

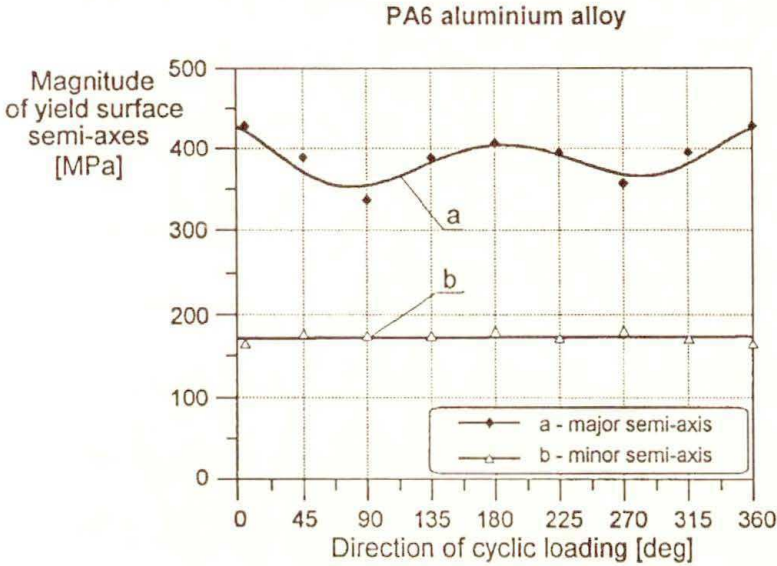


FIG. 19. Variations of the major and minor semi-axes of subsequent yield surfaces for the aluminium alloy.

Completely opposite effects were observed for the aluminium alloy, Fig. 19. The material generally exhibits a hardening effect. Although for the directions coincident with cyclic loading the maximum hardening was observed, the degree of this effect was not the same for all the directions considered. It is interesting to note that for the aluminium alloy there were no clear differences in the magnitude of minor axes of the subsequent yield surfaces. The reason of such behaviour results from the manufacturing processes used to produce rods of aluminium alloy. These processes induced anisotropy which could not be changed by the cyclic loading applied in the experimental programme.

In Fig. 19 it is also easy to find a confirmation of the conclusion that for the selected proportional cyclic loading path the degree of hardening was almost not sensitive to the sense of loading. For example, the degree of hardening for the tension-compression direction was almost the same (the difference was less than 5%), independently of the sense of the cyclic process initiation, i.e. the tension (0°) or the compression (180°).

It is interesting to study how cyclic deformation influences the rotation of yield surfaces. In the case of steel tested, the rotation depends on the cyclic loading path. Experimental data illustrating the rotation of the initial yield locus due to cyclic loading path orientation are shown in Fig. 20 in form of circles for the steel, and crosses for the aluminium alloy. Lines in this figure correspond to the approximations carried out using the least squares method. A significant rotation of the yield surface is observed for the steel. It depends on the orientation of the cyclic loading path. However, as it is shown in Fig. 20, the angle of rotation of the yield surface almost does not depend on the sense of loading. It means that there are no significant differences in rotation for cyclic loading determined by those ϕ which describe the same direction, that is 0° and 180° , 45° and 225° , 90° and 270° , 135° and 315° .

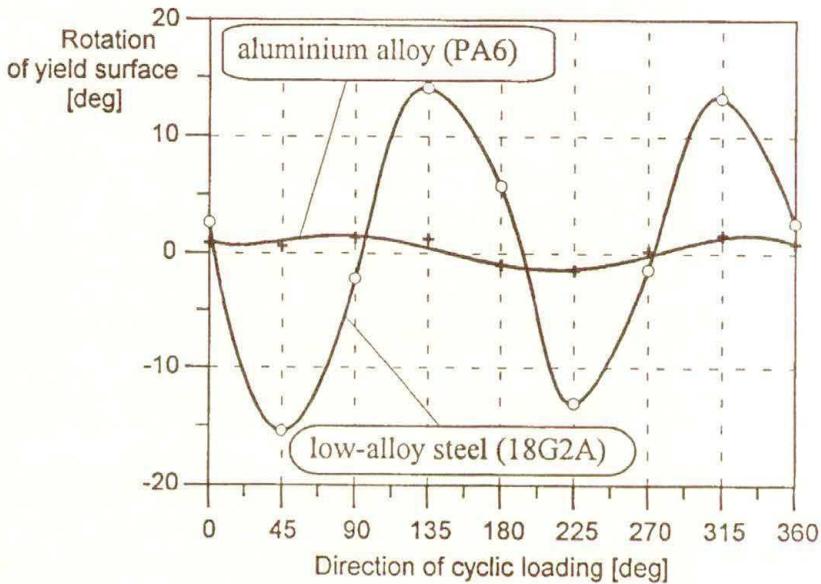


FIG. 20. Comparison of the yield surfaces rotation due to cyclic prestraining.

In the case of aluminium alloy the results show an opposite effect, that is there was not observed any significant rotation of the subsequent yield surfaces due to the same programme of cyclic loading as that applied during the steel tests.

In order to complete the analysis of both materials, in Figs. 21 and 22 are presented the variations of yield limits due to cyclic prestraining for the low-alloy steel and aluminium alloy, respectively. Initial values of the yield limits obtained for the same offset strain equal to 5×10^{-5} are shown in Table 3 for the low-alloy steel and in Table 4 for the aluminium alloy.

Table 3. Yield limits for the as-received low-alloy steel (offset strain 5×10^{-5}).

Tension yield limit	Compression yield limit	Torsion yield limit	Reverse torsion yield limit
372 MPa	280 MPa	198 MPa	210 MPa

Table 4. Yield limits for the as-received aluminium alloy (offset strain 5×10^{-5}).

Tension yield limit	Compression yield limit	Torsion yield limit	Reverse torsion yield limit
341 MPa	341 MPa	150 MPa	150 MPa

All yield limits considered for the steel decreased after cyclic prestraining. Maximum decreasing of the corresponding yield limits was obtained for the directions coincident with cyclic loading. As shown in Fig. 21, the tension and

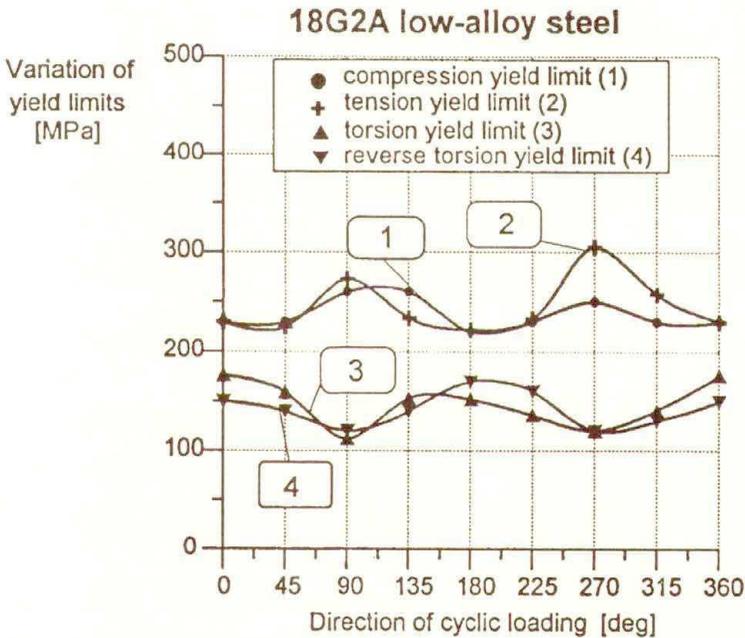


FIG. 21. Variations of yield limits due to cyclic prestraining of the steel.

compression yield limits do not differ considerably after prestraining. Since these parameters before cyclic loading differ by more than 20%, it can be concluded

that the process of cyclic prestraining caused forgetting of the initial anisotropy resulting from the manufacturing processes of rods used as the blanks for specimens.

In the case of the aluminium alloy, almost all yield limits increased (except the tension yield limits for the directions of cyclic loading described by the value of ϕ equal to 45° , 90° and 135°) after cyclic loading in comparison to those determined for the material in the as-received state. Contrary to the steel, the torsion and reverse torsion yield limits for the aluminium alloy after prestraining do not depend on the cyclic loading direction. For all directions the same values of these limits were obtained and they can be approximated with a good accuracy by straight lines, Fig. 22. Such a result suggests that the range of strain realised during cyclic loading was not sufficient to change the initial anisotropy of the aluminium alloy, and the material still exhibits a memory for the maximum prestress induced during the manufacturing processes.

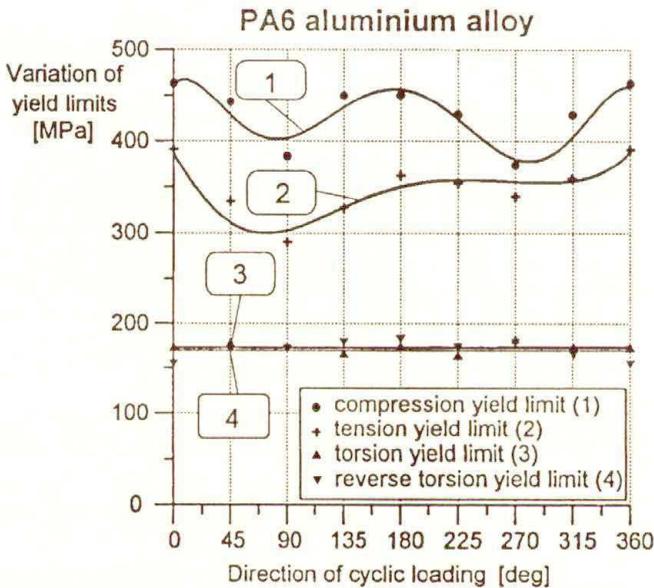


FIG. 22. Variations of yield limits due to cyclic prestraining of the aluminium alloy.

6. Applicability assessment of the cyclic yield surface concept

Having cyclic curves and the results from monotonic loading tests used to obtain subsequent yield surfaces for the materials tested after prestraining, the directions of maximum softening/or hardening due to cyclic loading can be identified in the strain range considered. It can be done using two methods. Using the first method, the cyclic yield surface shown earlier, can be constructed on the basis of cyclic curves.

In the second method, a surface being an envelope of all yield loci determined for the cyclically prestrained material can be constructed. Such a surface can be obtained on the basis of stress-strain diagrams coming from the first probes of the single-specimen method used to determine the subsequent yield surfaces. To construct this surface, the results obtained from eight first probes were used. Since each time the first probe was taken to be coincident with the direction of the first cyclic loading, the experimental programme for both materials enables us to determine eight points creating the envelope mentioned above. Assuming the yield offset to be $\varepsilon_{\text{off}} = 5 \times 10^{-5}$, the surfaces being envelopes of all subsequent yield loci presented in Fig. 14 for the aluminium alloy and in Fig. 16 for the steel, can be constructed. In the case of steel, the surface obtained in this way represents the maximum softening of the material. In Fig. 23 it is compared with the cyclic

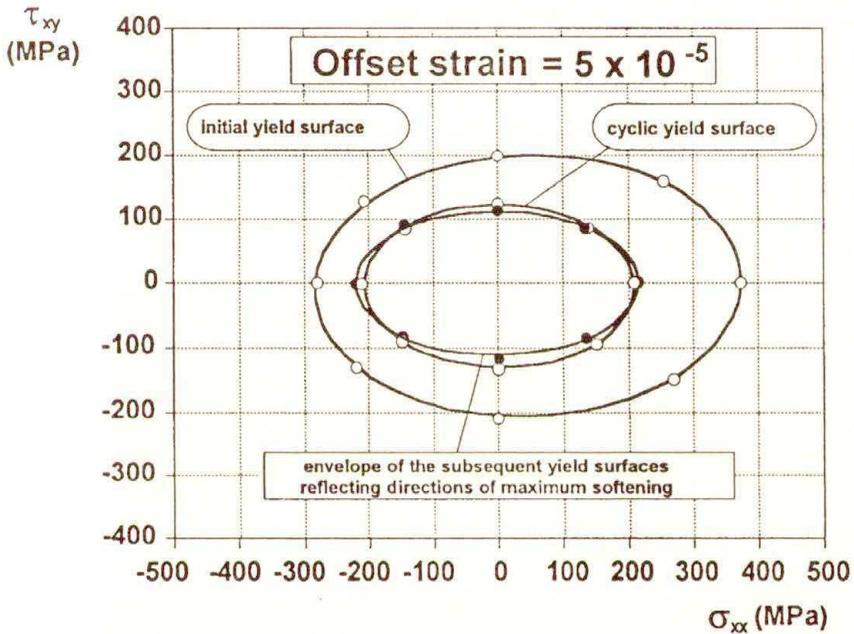


FIG. 23. Comparison of the envelope of subsequent yield surfaces, reflecting directions of maximum material softening due to cyclic loading, with the cyclic yield surface, offset strain 5×10^{-5} (results for the steel).

yield surface determined on the basis of cyclic curves, Fig. 12, and with the initial yield locus. As it is clearly shown, a close agreement was achieved in locations and sizes between the cyclic yield surface and the envelope. Thus, it confirms the equivalence and applicability of both methods of mechanical properties analysis for the steel subject to prior cyclic deformation in the plane stress state.

In the case of aluminium alloy, the surface being an envelope of all subsequent yield loci is shown in Fig. 24.

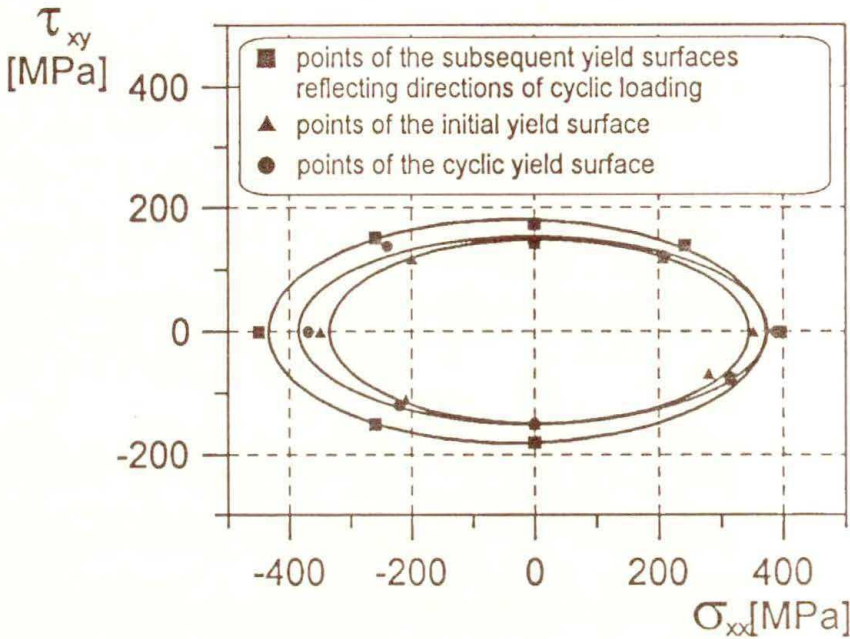


FIG. 24. Comparison of the envelope of subsequent yield surfaces, reflecting directions of maximum material hardening due to cyclic loading, with the cyclic yield surface, offset strain 5×10^{-5} (results for the aluminium alloy).

It is compared with the cyclic yield locus as well as with the initial yield surface. Contrary to the steel specimens, significant differences can be observed between the cyclic yield surface and the envelope. In view of this, the question arises why for one material a close agreement can be achieved between the cyclic yield surface and the envelope, but for the others considerable discrepancies are observed? In order to explain this problem, we must return to the results concerning cyclic loading. It has been shown for the aluminium alloy that the saturation cycle was not achieved during cyclic loading with the constant strain amplitude. The results for steel indicate that in order to obtain the saturation cycle, only a few full cycles with constant strain amplitude were necessary. It seems that the lack of stable behaviour of the aluminium alloy during cyclic loading applied is the main reason for the differences between the cyclic yield surface and the envelope. Therefore, it can be stated that the applicability of the cyclic yield surface concept to the mechanical properties analysis is limited to those cases in which the material tested reaches the stable hysteresis loop during proportional cyclic loading.

7. Final remarks

Determination of the true constitutive equations for cyclic plasticity provides many difficulties since, up to now, the majority of experimental investigations have been carried out at uniaxial stress states. Therefore, the available experimental data for multiaxial stress conditions are limited and, as a consequence, they do not fully reflect all aspects of the material behaviour under cyclic loadings. Since the paper presents the results of tests carried out under complex stress state, it completes somehow the lack of data in this area and may be useful in modelling the material behaviour. The data obtained allow us to formulate a few important concluding remarks.

It was observed that the shape and location of the initial yield surfaces determined for both the aluminium alloy and steel, for clearly defined yield offset, identify the anisotropy of the materials coming from the manufacturing processes.

A cyclic loading programme induces softening of the steel in the considered strain range accompanied by a remarkable reduction of the yield loci dimensions. In the case of aluminium alloy, the same programme induces the hardening effect reflected by the increase of yield loci dimensions.

The amount of softening in the case of steel, and hardening in the case of aluminium alloy depends on the direction with respect to cyclic prestraining. The greatest effects were always observed in the same direction as that used during predeformation process whereas the smallest ones were observed in the direction perpendicular to that in the cyclic loading applied.

If the number of cycles is sufficient to achieve the state of saturation, the concept of the cyclic yield surface reflects well the ability of a material to change mechanical properties due to cyclic deformation in different orientations of the plane stress state.

The analysis of the dimensions of the cyclic yield surface for the 18G2A steel proves that the material exhibits the same softening level for all directions examined, and moreover, it forgets the initial anisotropy induced during strain history coming from the manufacturing processes. The same analysis for the aluminium alloy proves that the material exhibits various amounts of hardening, depending on the initial anisotropy.

Acknowledgement

The authors gratefully acknowledge the support of the State Committee for Scientific Research under Grant 3 0154 91 01.

References

1. J. D. MORROW, *Cyclic plastic strain energy and fatigue of metals, internal friction, damping and cyclic plasticity*, ASTM STP 378, American Society for Testing and Materials, 45–87, 1965.
2. P. W. LANDGRAF, J. D. MORROW, T. ENDO, *Determination of the cyclic stress-strain curve*, J. Materials, **4**, 176–188, 1969.
3. E. KREMPL, *Cyclic plasticity: Some properties of the hysteresis curve of structural metals at room temperature*, ASME Journal of Basic Engineering, **93**, 317–323, 1971.
4. R. MARJANOVIC, W. SZCZEPIŃSKI, *Yield surfaces of the M-63 brass prestrained by cyclic biaxial loading*, Arch. Mech., **26**, 311–320, 1974.
5. J. LIPKIN, J. C. SWEARENGEN, *On the subsequent yielding of an aluminium alloy following cyclic prestraining*, Metallurgical Transactions A, **6A**, 167–177, 1975.
6. J. MIASTKOWSKI, *Yield surface of material subjected to combined cyclic loading*, Arch. Mech., **30**, 203–215, 1978.
7. H. S. LAMBA, O. M. SIDEBOTTOM, *Proportional biaxial cyclic hardening of annealed oxygen-free high-conductivity copper*, Journal of Testing and Evaluation, **6**, 260–267, 1978.
8. H. S. LAMBA, O. M. SIDEBOTTOM, *Cyclic plasticity for nonproportional paths*, ASME J. Engng. Materials and Technology, **100**, 96–111, 1978.
9. E. TANAKA, S. MURAKAMI, M. OOKA, *Effects of plastic strain amplitudes on non-proportional cyclic plasticity*, Acta Mechanica, **57**, 167–182, 1985.
10. E. TANAKA, S. MURAKAMI, M. OOKA, *Effects of strain path shapes on non-proportional cyclic plasticity*, J. Mech. Phys. Solids, **33**, 559–575, 1985.
11. D. L. MCDOWELL, *A two-surface model for transient nonproportional cyclic plasticity*, ASME J. App. Mech., **52**, 298–308, 1985.
12. CHR. BOLLER, T. SEEGER, *Materials data for cyclic loading. Part A: Unalloyed steels* (Materials Science Monographs, 42A), Amsterdam – Oxford – New York – Tokyo, Elsevier 1987.
13. W. TRĄMPCZYŃSKI, *The experimental verification of the evolution of kinematic and isotropic hardening in cyclic plasticity*, J. Mech. Phys. Solids, **36**, 417–441, 1988.
14. A. BENALLAL, P. LEGALLO, D. MARQUIS, *An experimental investigation of cyclic hardening of 316 stainless steel and 2024 aluminium alloy under multiaxial loadings*, Nucl. Eng. Des., **114**, 345–353, 1989.
15. E. KREMPL, H. LU, *The path and amplitude dependence of cyclic hardening of type 304 stainless steel at room temperature*, [in:] *Biaxial and Multiaxial Fatigue*, M. W. BROWN, K. J. MILLER [Eds.], 89–106, Mechanical Engineering Publications, London 1989.
16. H. ISHIKAWA, K. SASAKI, *Stress-strain relations of SUS304 stainless steel after cyclic preloading*, ASME J. Engng. Materials and Technology, **111**, 417–423, 1989.
17. Z. L. KOWALEWSKI, M. ŚLIWOWSKI, *Effect of cyclic loading on the yield surface evolution of 18G2A low-alloy steel*, Int. J. Mech. Sci., **39**, 1, 51–68, 1997.
18. Z. L. KOWALEWSKI, *Assessment of cyclic properties of 18G2A low-alloy steel at biaxial stress state*, Acta Mechanica, **120**, 1–4, 71–90, 1997.
19. Z. L. KOWALEWSKI, *Effect of cyclic prestraining on plastic behavior of 18G2A low-alloy steel at complex stress state*, Proc. of Plasticity: The Sixth Int. Symp. on Plasticity and Its Current Applications, A. S. KHAN [Ed.], Juneau, Alaska, USA, July 14–18, 359–360, 1997.

20. R. V. MISES, *Mechanik der plastischen Formänderung von Kristallen*, Zeitschr. Angew. Math. Mech., **8**, 161–185, 1928.
21. W. SZCZEPIŃSKI, *On deformation-induced plastic anisotropy of sheet metals*, Arch. Mech., **45**, 3–38, 1993.

POLISH ACADEMY OF SCIENCES
INSTITUTE OF FUNDAMENTAL TECHNOLOGICAL RESEARCH
e-mail: ldietric@ippt.gov.pl
e-mail: zkowale@ippt.gov.pl

Received March 26, 1998.
